

## Toward complete spectroscopy using $\beta$ decay: The example of $^{32}\text{Cl}(\beta\gamma)^{32}\text{S}$

E. Aboud,<sup>1,2,\*</sup> M. B. Bennett,<sup>1,2,3,†</sup> C. Wrede,<sup>1,2,‡</sup> M. Friedman,<sup>2</sup> S. N. Liddick,<sup>2,4</sup> D. Pérez-Loureiro,<sup>1,2</sup> D. W. Bardayan,<sup>5</sup> B. A. Brown,<sup>1,2</sup> A. A. Chen,<sup>6</sup> K. A. Chippis,<sup>7,8</sup> C. Fry,<sup>1,2,3</sup> B. E. Glassman,<sup>1,2</sup> C. Langer,<sup>2,3</sup> E. I. McNeice,<sup>6</sup> Z. Meisel,<sup>1,2,3</sup> W.-J. Ong,<sup>1,2,3</sup> P. D. O'Malley,<sup>5</sup> S. D. Pain,<sup>7</sup> C. J. Prokop,<sup>2,4</sup> H. Schatz,<sup>1,2,3</sup> S. B. Schwartz,<sup>1,2,9</sup> S. Suchyta,<sup>2,4</sup> P. Thompson,<sup>7,8</sup> M. Walters,<sup>6</sup> and X. Xu<sup>1,2</sup>

<sup>1</sup>Department of Physics and Astronomy, Michigan State University, East Lansing, Michigan 48824, USA

<sup>2</sup>National Superconducting Cyclotron Laboratory, Michigan State University, East Lansing, Michigan 48824, USA

<sup>3</sup>Joint Institute for Nuclear Astrophysics, Michigan State University, East Lansing, Michigan 48824, USA

<sup>4</sup>Department of Chemistry, Michigan State University, East Lansing, Michigan 48824, USA

<sup>5</sup>Department of Physics, University of Notre Dame, Notre Dame, Indiana 46556, USA

<sup>6</sup>Department of Physics and Astronomy, McMaster University, Hamilton, Ontario L8S 4M1, Canada

<sup>7</sup>Oak Ridge National Laboratory, Oak Ridge, Tennessee 37831, USA

<sup>8</sup>Department of Physics and Astronomy, University of Tennessee, Knoxville, Tennessee 37996, USA

<sup>9</sup>Department of Geology and Physics, University of Southern Indiana, Evansville, Indiana 47712, USA



(Received 30 March 2018; published 15 August 2018)

**Background:**  $^{32}\text{Cl}$  is a neutron-deficient isotope with a  $\beta$ -decay half-life of 298 ms and a spin and parity of  $J^\pi = 1^+$ . Previous measurements of  $^{32}\text{Cl}$   $\beta$ -delayed  $\gamma$  rays have yielded a  $\beta$ -decay scheme with twelve  $\beta$ -decay transitions, contributing to studies of nuclear structure and fundamental symmetries. Those experiments have been limited to the observation of  $^{32}\text{S}$  states with  $J^\pi = 0^+, 1^+, 2^+$ .

**Purpose:** Our goal is to search for new  $\beta$ -delayed  $\gamma$  rays and  $\beta$ -decay transitions of  $^{32}\text{Cl}$  to  $^{32}\text{S}$ .

**Methods:** A measurement of  $^{32}\text{Cl}$   $\beta$ -delayed  $\gamma$  decay has been performed using the Clovershare array of high-purity germanium detectors at the National Superconducting Cyclotron Laboratory.

**Results:** By acquiring the highest-statistics  $^{32}\text{Cl}$   $\beta$ -delayed  $\gamma$ -ray spectrum to date and exploiting a new sensitivity to  $\gamma$ - $\gamma$  coincidences, this experiment has enabled the observation of nine previously unobserved  $\beta$ -delayed  $\gamma$ -ray transitions, leading to the inference of five  $\beta$ -decay transitions never before observed in  $^{32}\text{Cl}$   $\beta$ -delayed  $\gamma$  decay. The set of observed states includes negative-parity states for the first time. By combining the new information with data from previous work, the lifetimes and partial widths of the 8861- and 9650-keV states of  $^{32}\text{S}$  have been determined. In addition, the  $^{31}\text{P}(p, \alpha)^{28}\text{Si}$  resonance strength of the 9650-keV state has been limited to  $\omega\gamma < 9.8$  meV, which is an improvement over direct measurements.

**Conclusion:** An enhanced decay scheme has been constructed. Most of the excited bound  $^{32}\text{S}$  states that would correspond to allowed and first-forbidden  $\beta$ -decay transitions have been observed, demonstrating the potential of  $\beta$ -decay experiments to approach complete spectroscopy measurements at the next generation of radioactive beam facilities. The observed positive-parity levels are well matched by  $sd$  shell-model calculations.

DOI: [10.1103/PhysRevC.98.024309](https://doi.org/10.1103/PhysRevC.98.024309)

### I. INTRODUCTION

Experimental studies of  $\beta^+$  decay in the  $sd$  shell are sensitive probes of nuclear structure that are applicable to searches for physics beyond the standard model of the electroweak interaction [1] and to the study of nucleosynthesis and energy generation in astrophysical hydrogen and helium burning environments [2–7]. In the past, the constraints imposed by  $\beta$ -decay selection rules, radioactive beam intensities, and radiation detection efficiencies have mostly limited the utility of  $\beta$ -decay spectroscopy to the study of the states whose population is allowed by the selection rules, except in special cases where

only forbidden transitions are energetically accessible. A good example is  $^{32}\text{Cl}$ : an unstable isotope [ $t_{1/2} = 298(1)$  ms,  $Q_{EC} = 12680.9(6)$  keV,  $J_{g.s.}^\pi = 1^+$ ] [8,9] that lies close to the valley of  $\beta$  stability and  $\beta^+$  decays to states in  $^{32}\text{S}$ , which has a stable ground state.

Early studies of  $^{32}\text{Cl}$  decay by Breckon *et al.* [10] and Glass *et al.* [11] tested the hypothesis that  $^{32}\text{Cl}$  was a part of a delayed heavy-particle emission series. Although they did not observe heavy-particle emission, they both reported four  $\beta$ -delayed  $\gamma$ -ray transitions; three  $\gamma$ -ray transitions were observed in common including the observation of decay from the first excited state of  $^{32}\text{S}$  via a  $\gamma$  ray of energy  $E_\gamma = 2230$  keV. In 1966 Anderson *et al.* [12] observed seven total  $\beta$ -delayed  $\gamma$  transitions, identifying the  $T = 1$  isobaric analog state (IAS) to have an excitation energy of 7014(10) keV. In 1968 Armini *et al.* [13] observed eight total  $\beta$ -delayed  $\gamma$  transitions with higher statistics than previous works, confirming the IAS and

\*abouderi@msu.edu

†benne438@msu.edu

‡wrede@nscl.msu.edu

providing the more precise energy of 6998(3) keV. Détraz *et al.* [14] observed twelve total  $\beta$ -delayed  $\gamma$  transitions, up to an energy of 7200 keV, and found the spin and parity of the newly observed 6666-keV state to be either  $1^+$  or  $2^+$ .

In the most recent literature on the  $\beta$  decay of  $^{32}\text{Cl}$ , Melconian *et al.* [15,16] reported the results of a precision experiment to improve  $\gamma$  yields and determine  $ft$  values. They observed every known excited  $^{32}\text{S}$  state that corresponds to an allowed  $\beta$ -decay transition up to the  $\alpha$ -particle emission threshold of 7 MeV. Their decay scheme pointed to isospin mixing between the  $1^+$  isobaric analog state at 7001.4(4) keV and the  $1^+$  state at 7190 keV and provided experimental information for 35  $\beta$ -delayed  $\gamma$  transitions up to 7200 keV. Their measurement demonstrated the largest isospin symmetry breaking effect in a superallowed Fermi  $\beta^+$  decay, providing an important test of nuclear structure corrections that are used in searches for new physics based on  $\beta^+$  decay [1,17]. Mixing of a similar magnitude has been observed in  $^{31}\text{S}$  using the  $\beta$  decay of another chlorine isotope,  $^{31}\text{Cl}$ , [6] and both cases have been explained in terms of  $T = 1$ ,  $J = 2$  isospin nonconserving interactions related to the  $s_{1/2}$  orbit [18]. Despite the relatively high sensitivity of their experiment, Melconian *et al.* were limited by a lack of statistics and acquisition of data at high  $\gamma$ -ray energies, and their decay scheme was consequently supplemented by including unobserved transitions adopted from experimental nuclear reaction data in the ENSDF database [8] and shell-model calculations. Only a single  $\gamma$ -ray detector was employed and  $\gamma$ - $\gamma$  coincidences could not be observed.

The present work further expands the  $\beta$ -delayed  $\gamma$ -decay scheme of  $^{32}\text{Cl}$  by acquiring the highest-statistics data set on this decay to date, providing sensitivity to new transitions and  $\gamma$ - $\gamma$  coincidence verification of the proposed decay scheme. The results are compared to the most recent experimental work [15,16] and to  $sd$  shell-model calculations. The new experimental information is also combined with information from other experiments to determine the previously unknown lifetimes of two  $^{32}\text{S}$  resonances and, in one case, to limit the strength of a  $^{31}\text{P}(p, \alpha)^{28}\text{Si}$  resonance at astrophysically relevant energies.

Generally, this work shows the potential of  $\beta$ -decay experiments to approach complete spectroscopy of energetically accessible nuclear states once next-generation radioactive ion beam facilities come online, despite the tendency of the  $\beta$ -decay process to selectively populate states with particular spins and parities.

## II. EXPERIMENT SETUP

The present measurement is part of a recent program of high-resolution  $\beta^+$ -delayed  $\gamma$ -decay measurements of proton-rich  $sd$ -shell nuclides [5–7,19–25]. The data set discussed in the present work was obtained over the course of approximately six hours at the National Superconducting Cyclotron Laboratory (NSCL) as calibration data for the analysis of an experiment designed to study the  $\beta$  decay of  $^{31}\text{Cl}$  [6,19,20].

The  $^{32}\text{Cl}$  production mechanism and experimental procedure are similar to those described in Refs. [6,19] for  $^{31}\text{Cl}$ . Briefly, a primary beam of 150-MeV/u, 75-p nA  $^{36}\text{Ar}$  was produced using the Coupled Cyclotron Facility at the NSCL

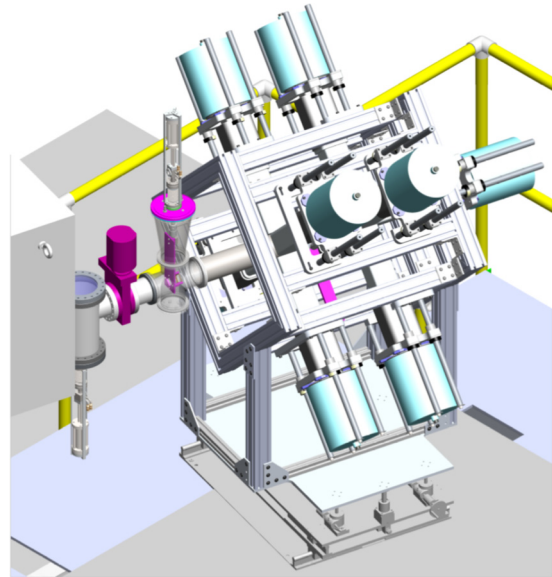


FIG. 1. Mechanical design drawing of the experimental apparatus used in the present work. The  $^{32}\text{Cl}$  beam enters from the left and is implanted into the scintillator (obscured) in the center of the Ge array. The  $\beta$ -delayed  $\gamma$  rays are detected by the nine surrounding high-purity Ge detectors, with eight detectors forming two rings around the scintillator and one detector along the beam axis. Each of the nine high-purity Ge detectors consists of four crystals.

and impinged upon a 1627-mg/cm<sup>2</sup> Be transmission target to generate a cocktail beam via projectile fragmentation that included  $^{32}\text{Cl}$ . Beam purification was accomplished both by using the A1900 fragment separator [26] with a 145-mg/cm<sup>2</sup> achromatic Al wedge and by time-of-flight separation using the Radio Frequency Fragment Separator (RFFS) [27]. Beam composition was sampled using the energy loss measurements in two 300- $\mu\text{m}$  Si semiconductor detectors, located approximately one meter upstream of the experimental setup. The time of flight over a 25 m path between a scintillator at the focal plane of the A1900 and the Si detectors was also used. Due to the high intensity of the  $^{32}\text{Cl}$  beam (max.  $3.3 \times 10^4$  pps), the Si detectors were inserted into the beamline only periodically to check the purity of the  $^{32}\text{Cl}$ , which was found to be consistently 99% pure, with only trace contaminants. While the Si detectors were in use, the beam intensity was attenuated to mitigate radiation damage to the detectors.

After passing through the RFFS, the  $^{32}\text{Cl}$  passed through a 3.8-cm-diameter collimator and was implanted into a 25-mm-thick plastic scintillator (BC408), that was optically coupled to a photomultiplier tube and used to record both the  $^{32}\text{Cl}$  implantations and the subsequent  $\beta$  decays of the ions.  $\beta$ -delayed  $\gamma$  rays were detected in the surrounding Yale Clovershare Array (Fig. 1), comprised of nine high-purity Ge detectors of four “clover” crystals each. The nine detectors were arranged in two rings of four detectors each: one ring on both the upstream and downstream side of the scintillator, with the ninth clover detector centered on the beam axis directly downstream of the scintillator. Signals from all 36 clover crystals, the scintillator,

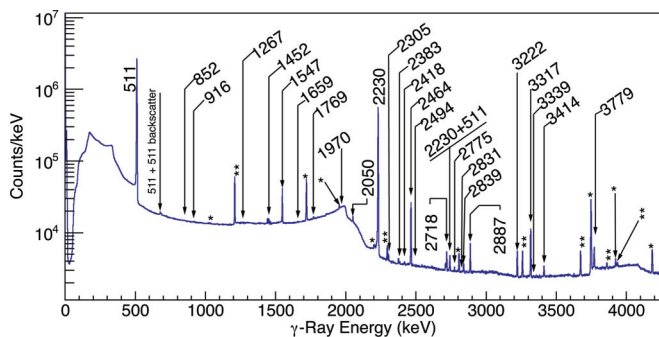


FIG. 2.  $^{32}\text{Cl}$   $\beta$ -delayed  $\gamma$ -decay spectrum gated on scintillator events.  $^{32}\text{S}$  peaks are labeled by  $\gamma$ -ray energy over the range of  $E_\gamma = 0$ –4250 keV. A single asterisk represents a first-escape peak and a double asterisk represents a second escape peak.

and Si detectors were processed using the NSCL Digital Data Acquisition System [28].

### III. ANALYSIS

In order to determine the  $\gamma$ -ray energies and intensities for the decay  $^{32}\text{Cl}(\beta^+\gamma)^{32}\text{S}$ , events were selected in a 1- $\mu\text{s}$  gate in the timing spectrum between signals in the scintillator and the germanium detectors. The timing gate allowed for  $^{32}\text{S}$   $\gamma$  rays in coincidence with a  $\beta$  particle to be counted preferentially while filtering out  $\gamma$  rays from room background and  $^{32}\text{Cl}$  that stopped in the collimator (Figs. 2 and 3). Each peak in the timing-gated and -ungated  $\gamma$ -ray energy histogram was fit with an exponentially modified Gaussian function superimposed on a localized linear background.

Low energy room background peaks were identified using compilations of common  $\gamma$ -ray room background lines [29]. For every peak, the ratio of the scintillator-gated to scintillator-ungated integral values was also taken. It was found that known peaks of  $^{32}\text{S}$  had a ratio of 60.2(1)% that was independent of  $\gamma$ -ray energy (and, inferentially, independent of  $\beta$ -decay endpoint energy) representing the efficiency of the scintillator to detect  $\beta$  particles from  $^{32}\text{Cl}$  decay in coincidence with  $^{32}\text{S}$   $\gamma$  rays in the clover array. While the intrinsic efficiency of the scintillator to detect  $\beta$  particles from the decays of implanted ions was effectively 100%, the lower ratio measured was attributed to ions that stopped in the collimator at the end

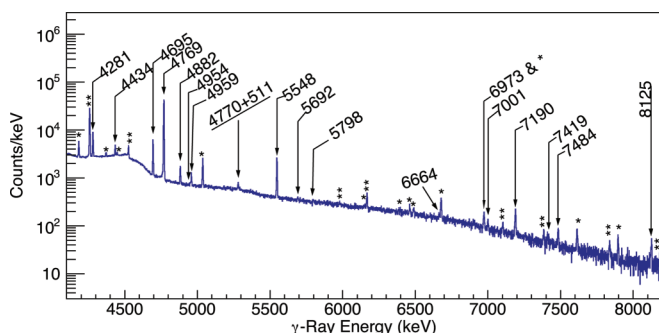


FIG. 3. Same as Fig. 2 for the  $\gamma$ -ray energy range of  $E_\gamma = 4100$ –8250 keV

of the beamline due to the finite size of the beam. The decays of those ions contributed to the Ge spectra, but were only registered in the scintillator with low efficiency. This ratio was used to help identify previously unobserved  $^{32}\text{S}$  photopeaks in the spectrum. 41 analyzed photopeaks along with the inference of three more photopeaks (Sec. III B 3) were determined to originate from  $^{32}\text{Cl}$   $\beta$ -delayed  $\gamma$ -ray transitions (Figs. 2, 3, and 4).

#### A. Energies

##### Energy calibration

To correct for the intrinsic differences in gain between the channels corresponding to each of the clover crystals used in the analysis, an energy calibration was performed, which was then used to determine the  $\gamma$ -ray energies. For every crystal, the individual energy histograms were calibrated internally using the  $^{32}\text{Cl}$   $\beta$ -delayed  $\gamma$ -ray energy values from Melconian *et al.* [15] as calibration standards up to 7190 keV. The spectra were summed to produce a single calibrated spectrum, incorporating all detectors for all runs. In part because the entirety of these data were taken over a short time span, it was found that gain drift over time was negligible for 31 of the crystals. The data from five crystals that displayed substantial gain drifts were not used in this analysis.

The statistical uncertainties for the energies were found by fitting the peaks with the exponentially modified Gaussian function and using the centroid as one of the free parameters. Each uncertainty was then inflated by the square root of the reduced chi-squared value for the corresponding fit. The systematic uncertainties for energies were constructed from, and dominated by, the energies and uncertainties documented by Melconian *et al.* [15] (Fig. 5).

#### B. Intensities

##### 1. $\gamma$ -ray efficiencies and $\gamma$ -ray intensities

The intensities were calibrated internally with respect to the standard intensities found by Melconian *et al.* [15]. We built a relative efficiency curve using  $^{152}\text{Eu}$  source data for  $E_\gamma < 1.4$  MeV and the normalized  $^{32}\text{Cl}(\beta^+\gamma)^{32}\text{S}$  photopeaks for  $1.5 < E_\gamma < 7.2$  MeV [6,19]. The relative efficiency curve was arbitrarily normalized to unity at 4281 keV and fit with the function

$$\epsilon = e^{-\sum p_i \log(E)^i}, \quad (1)$$

where  $\sum p_i \log(E)^i$  was a sixth-degree polynomial of  $\log(E)$ . The degree of the fit was determined by adding terms to the sum until a good fit ( $\chi^2/\nu = 0.51$ ,  $p = 0.87$ ) was obtained. This function was used to interpolate the measured relative efficiencies and extrapolate them up to 8.2 MeV.

The uncertainties were determined by the same methods described by Bennett *et al.* [6,19] and included a 1% uncertainty associated with  $\gamma$ - $\gamma$  summing effects. For  $E_\gamma < 1.5$  MeV, the dominant systematic uncertainty was the summing effect for the  $^{152}\text{Eu}$  data. The dominant systematic uncertainty for  $E_\gamma > 1.5$  MeV was the error envelope adopted from Melconian *et al.* [15] The total uncertainty envelope of the relative efficiency curve is presented in Fig. 6.

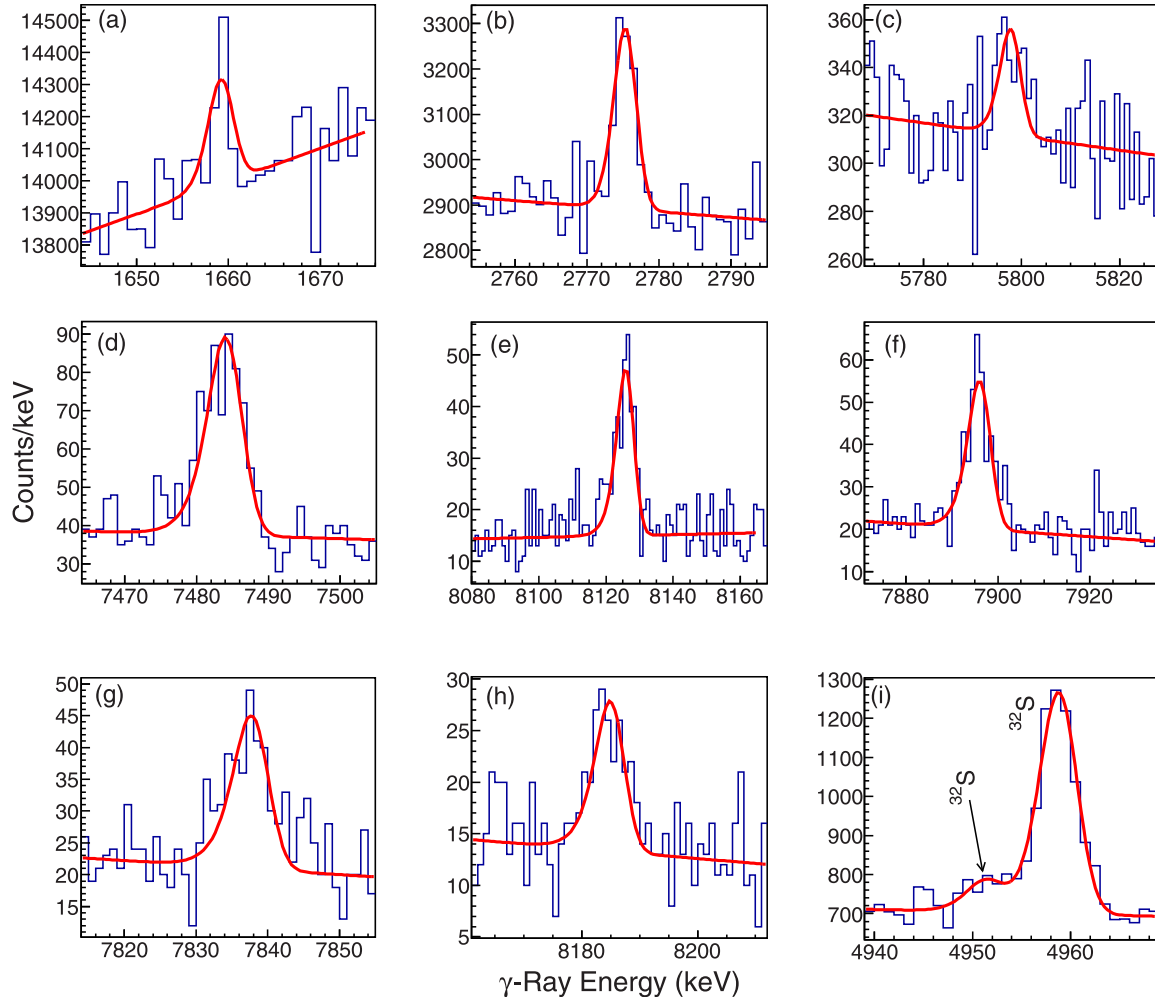


FIG. 4. Nine segments of the histogram in Figs. 2 and 3 displaying the peaks corresponding to the previously unobserved  $\gamma$  rays presented in this analysis (blue online) and the corresponding fits (red online). (a) The 1659-keV photopeak, which corresponds to decays from the  $2^+$  state at 6666 keV to the  $3^-$  state at 5006 keV. (b) The 2775-keV photopeak, which corresponds to decays from the  $3^-$  state at 5006 keV. (c) The 5798-keV photopeak. (d) The 7484-keV photopeak. (e) The 8125-keV photopeak. (f) The first-escape peak at 7895 keV that was used, following the procedure described in Sec. III B 3, to determine the intensity of the 8407-keV photopeak. (g) The second escape peak at 7839 keV that was used to determine the intensity of the 8861-keV photopeak. (h) The second escape peak at 8186 keV that was used to determine the intensity of the 9207-keV photopeak. (i) Both the 4954-keV and 4959-keV photopeaks. The 4954-keV photopeak is newly observed, while the 4959-keV photopeak was observed in previous experiments.

## 2. GEANT4 simulations

We also used the GEANT4 Monte Carlo software package [30] to simulate the efficiency of the germanium array at each of the energies used in the calibration by incorporating the gross features of the experimental geometry. The GEANT4 efficiency curve was found to produce accurate relative efficiencies when compared to the data, validating certain aspects of the simulation for an application described in the following subsection.

## 3. Peaks above the detection energy threshold

In several cases, high-energy escape peaks were observed corresponding to photopeaks that were not observed because they were above the upper energy threshold of 8200 keV set for the data acquisition (optimized for the  $^{31}\text{Cl}$  experiment). By calibrating the ratio of the integral value of both the first

and second escape peaks to that of the corresponding observed photopeaks, the intensities of unobserved photopeaks were inferred using only the escape peaks. Plotting this ratio as a function of energy (Fig. 7) allowed us to extrapolate to  $\gamma$ -ray energies above 8200 keV. Both the first and second escape peak ratio curves could be adequately fit using linear functions with respect to energy. This procedure was used to find the intensities for the transitions at energies of 8407, 8861, and 9207 keV. The escape peak to photopeak ratios were simulated for the same peaks using GEANT4 [30] and a consistent linear shape was found, corroborating the semiempirical values. To account for systematic uncertainties two alternative extrapolations were applied: (1) the data points were fit with a second-degree polynomial and (2) the highest energy data points were fit with the linear function used to fit the GEANT4 data points. By taking the average of the deviation from both

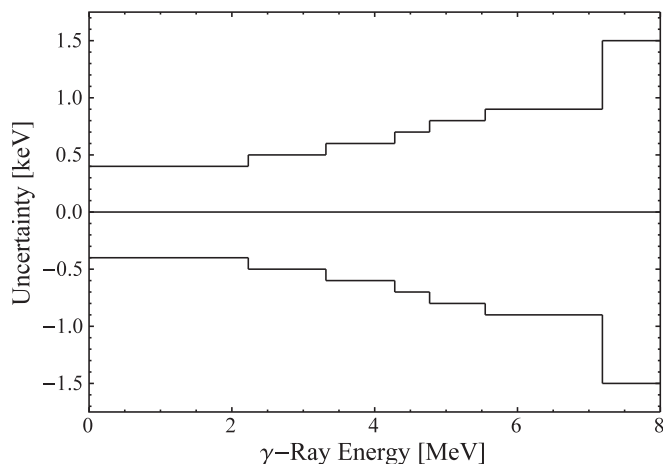


FIG. 5. Systematic uncertainty envelope for the determination of  $\gamma$ -ray energies constructed from the calibration standards adopted from [15].

methods, the systematic uncertainty was determined to be 14% at the maximum energy considered.

#### 4. $\gamma$ -decay probabilities and $\beta$ -decay probabilities

$\gamma$ -decay transition probabilities for  $^{32}\text{S}$  levels were found by calculating the ratio of individual  $\gamma$ -ray intensities (Sec. III B 1) decaying from a given  $^{32}\text{S}$  state to the sum of the  $\gamma$ -ray intensities for transitions decaying from that  $^{32}\text{S}$  state.

The intensity of the  $^{32}\text{Cl}$   $\beta$ -decay transition to each  $^{32}\text{S}$  state was calculated from the difference between the feeding and decaying  $\gamma$ -ray intensities. For the 8861- and 9650-keV  $^{32}\text{S}$  states the  $\beta$ -delayed proton and  $\alpha$ -particle emission branches from Honkanen *et al.* [31] were added to the  $\beta$ -delayed  $\gamma$ -

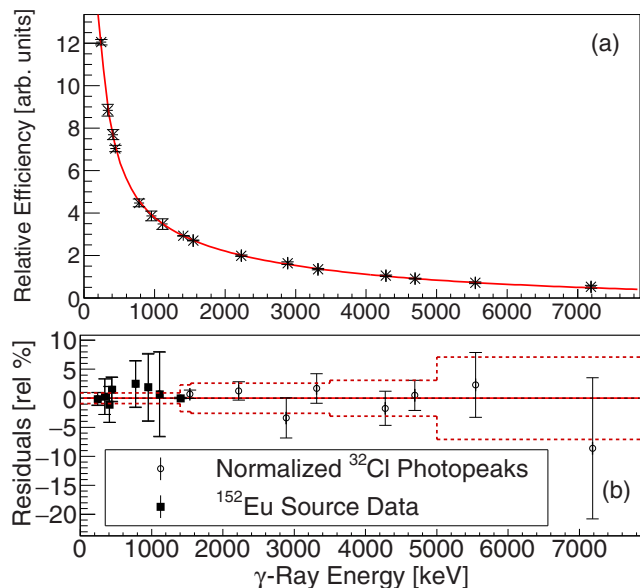


FIG. 6. (a) Relative  $\gamma$ -ray efficiency curve for the Clovershare array. (b) Residuals between the plotted functional form of the efficiency curve and the data points. The error envelope of the relative efficiencies is plotted, as a dashed line, on the residual plot.

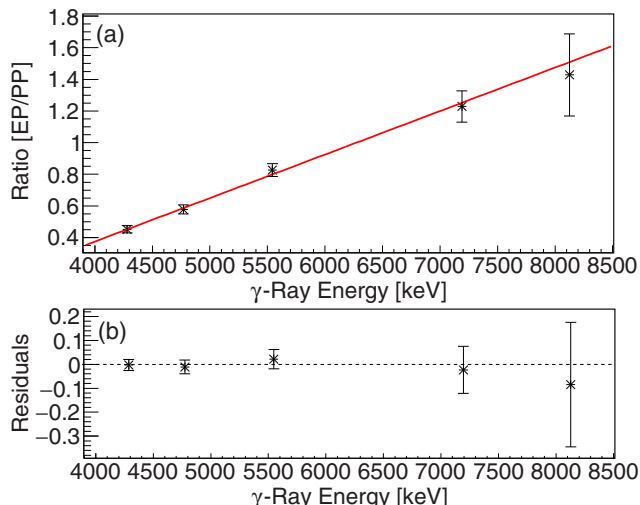


FIG. 7. (a) Ratio of the second escape peak integral value (EP) to the photopeak integral value (PP). The plot was fit with a linear function, ( $\chi^2/\nu = 0.18$ ). (b) Residuals of the linear fit.

decay branches from the present work to calculate the  $\beta$ -decay intensities, giving a total  $\beta$ -decay intensity for each of these two  $^{32}\text{S}$  states. Unobserved  $^{32}\text{S}$   $\gamma$ -decay branches that are known from previous nuclear reaction data [8] were also included.

#### 5. Upper limits

We set upper limits for the intensities of selected unobserved  $\gamma$ -ray transitions for comparison to previous work. Using the photopeak integral values (consistent with zero), and the respective uncertainties, of unobserved  $\gamma$  rays the upper limits of their intensities were found at a 90% confidence level. Each upper limit was normalized to the intensity of the strongest branch from the respective state.

#### 6. $ft$ values

The  $\log(ft)$  values were calculated for each allowed  $\beta$ -decay transition. The  $\beta$ -decay branches deduced from the present work were used as input along with the known  $^{32}\text{Cl}$  half-life. Values for the phase space factor  $f$  were adopted from Ref. [15] when available; otherwise the procedures described in Ref. [32] were employed (those two calculations of  $f$  agreed to within a few percent).

#### C. $\beta$ - $\gamma$ coincidences

The high granularity of the Yale Clovershare Array allowed us to construct  $\beta$ - $\gamma$ - $\gamma$  coincidence spectra, providing supporting evidence for the proposed decay scheme. To account for random coincidences and Compton background, each coincidence spectrum was compared to a corresponding histogram (e.g., Fig. 9) that was gated on the background near the peak of the coincidence gate in the energy spectrum. A  $3\sigma$  statistical significance was chosen as a threshold for positive detection of coincidences and it was also possible to detect most of those by back-gating. Table I presents a matrix of  $\gamma$ -ray transitions that were found to be in coincidence.

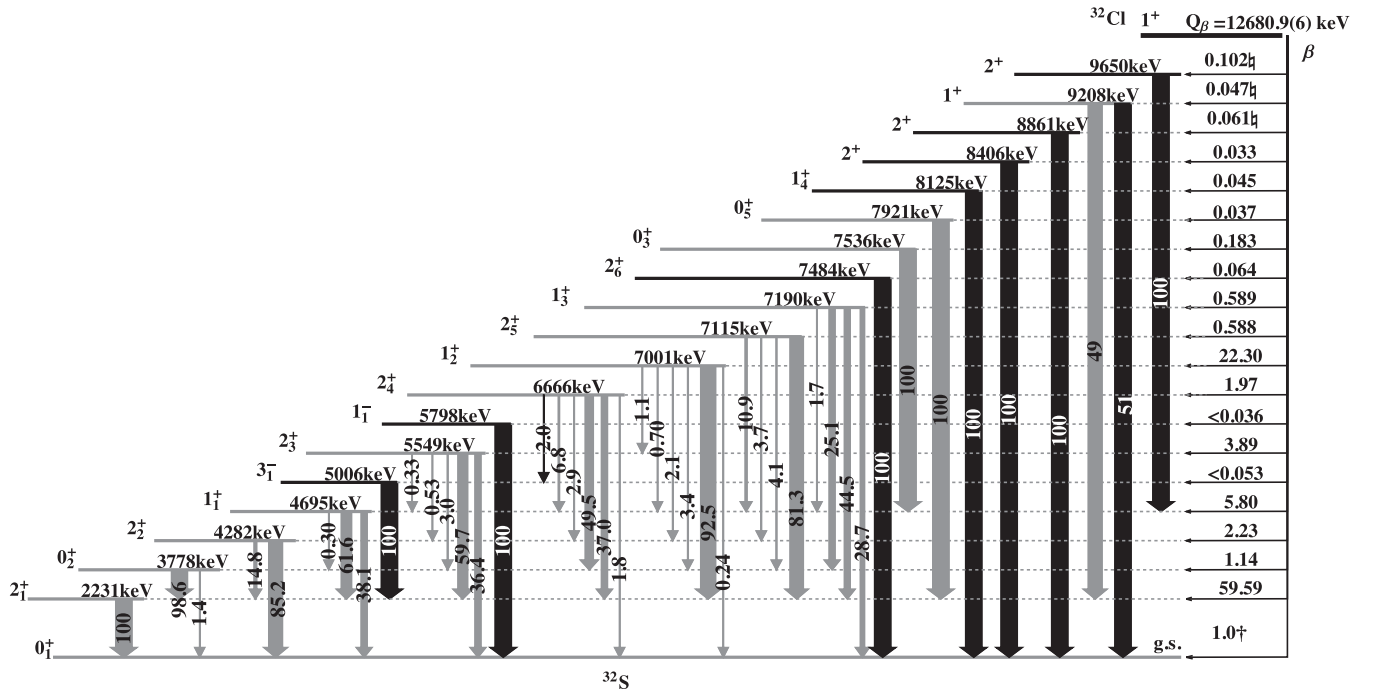


FIG. 8.  $^{32}\text{Cl}$   $\beta$ -delayed  $\gamma$ -decay scheme derived from the present work. Energy levels and transitions shown in gray represent previously known states and decays. Energy levels and transitions shown in black represent states and decays observed in the present work for the first time from the  $\beta$  decay of  $^{32}\text{Cl}$ . The  $\beta$ -decay feeding values are shown to the right of the  $^{32}\text{S}$  energy states.  $\beta$ -decay intensities are shown in percent of  $^{32}\text{Cl}$  decays,  $\gamma$ -decay probabilities are shown in percent of  $\gamma$  decays from the respective state, and their values and uncertainties can be found in Table IV. The  $\beta$  transition labeled with † was adopted from Armini *et al.* [13] and the ones labeled with ‡ include  $\beta$ - $\alpha$ ,  $\beta$ - $p$ , and  $\beta$ - $\gamma$  branches from ENSDF [8]. The energy levels are not plotted to scale, but simply increasing incrementally.

#### D. Spins and parities

In addition to the analysis of the experimental data acquired in the present work, the results were compared to theoretical  $sd$  shell-model calculations (detailed in Sec. IV C) of  $ft$  values for  $^{32}\text{Cl}$   $\beta$ -decay transitions and  $\gamma$ -decay transition probabilities of  $^{32}\text{S}$  states (Table III and Fig. 10). By comparing these detailed feeding and decay properties, each positive parity  $^{32}\text{S}$  state

observed up to 8 MeV could be matched with a shell-model state, providing spin and parity arguments for those states.

#### E. Resonance widths and lifetimes of states

For a few unbound  $^{32}\text{S}$  states that were observed in the present work via  $\beta$ -delayed  $\gamma$  decay and also observed in previous work via  $\beta$ -delayed particle emission and radiative capture reactions, the partial widths  $\Gamma_\gamma$ ,  $\Gamma_p$ , and  $\Gamma_\alpha$  and lifetimes  $\tau$  could be determined. The general procedure was to (1) supplement the observed  $\beta$ -delayed  $\gamma$ -decay branch using other known  $\gamma$ -decay branches of the state to determine the total  $\beta$ -delayed  $\gamma$  intensity through the state; (2) compare the total  $\beta$ -delayed  $\gamma$ -decay intensity through the state with the total  $\beta$ -delayed particle intensity through the state in order to determine the branching ratios  $\Gamma_\gamma/\Gamma$ ,  $\Gamma_p/\Gamma$ , and  $\Gamma_\alpha/\Gamma$ ; (3) combine the branching ratios with radiative capture resonance strengths and spins from the literature to calculate the total width,  $\Gamma$ , of the state; (4) invert the width to determine the lifetime; and (5) combine the total width with the branching ratios to determine the partial widths. In one case the deduced partial widths were applied to calculate the strength of a  $^{31}\text{P}(p, \alpha)^{28}\text{Si}$  resonance at astrophysically relevant energies.

### IV. RESULTS AND DISCUSSION

#### A. Overview

In the present work nine new  $^{32}\text{Cl}$   $\beta$ -delayed  $\gamma$ -ray transitions were observed leading to the inference of five  $\beta$ -decay

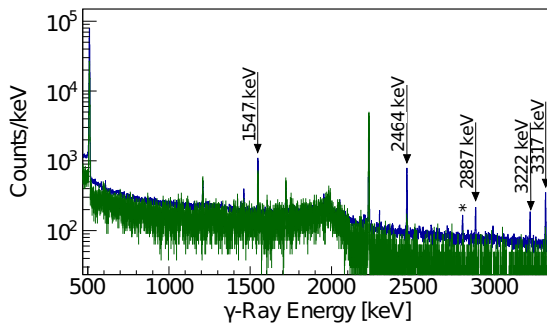


FIG. 9. The  $\beta$ - $\gamma$ - $\gamma$  coincidence spectrum for the 2230-keV gate. The darker (blue online) histogram is the coincidence spectrum and the lighter (green online) histogram was obtained by gating on the background in the  $\gamma$ -ray energy spectrum near the 2230-keV peak. The labeled peaks correspond to  $^{32}\text{S}$   $\gamma$ -ray transitions found to be in coincidence with the 2230-keV  $\gamma$ -ray. The single asterisk represents a first-escape peak.

TABLE I.  $\beta$ - $\gamma$ - $\gamma$  coincidence matrix. The column and row headings list the energies of  $\gamma$  rays (keV) for which at least one other  $\gamma$  ray was observed in coincidence with a statistical significance  $\geq 3\sigma$ . A check mark indicates an observed coincidence, the symbol “-” indicates no coincidence observed and a blank entry represents the fact that a gamma ray transition cannot be observed in coincidence with itself.

	1547	2050	2230	2464	2775	3317	4281	4694	5548
852	-	-	-	✓	-	-	-	✓	-
916	✓	-	-	-	-	-	-	-	-
1267	-	-	-	-	-	-	✓	-	-
1452	-	-	-	-	-	✓	-	-	✓
1547	-	-	✓	-	-	-	-	-	-
1659	-	-	-	-	✓	-	-	-	-
1769	✓	-	-	-	-	-	-	-	-
1970	-	-	-	✓	-	-	-	-	-
2230	✓	-	-	✓	-	✓	✓	-	-
2305	-	-	-	✓	-	-	-	-	-
2464	-	-	✓	-	-	-	-	-	-
2719	-	✓	-	-	-	-	✓	-	-
2839	-	-	-	✓	-	-	-	✓	-
2887	✓	-	✓	-	-	-	-	-	-
3222	✓	-	✓	-	-	-	-	-	-
3317	-	-	✓	-	-	-	-	-	-
4434	-	-	✓	-	-	-	-	-	-
4769	-	-	✓	-	-	-	-	-	-
4882	-	-	✓	-	-	-	-	-	-
4959	-	-	✓	-	-	-	-	-	-

branches that have not been observed in  $^{32}\text{Cl}$   $\beta$ -delayed  $\gamma$  decay before. Three of the  $\beta$ -decay transitions have never been observed in  $\beta$ -delayed particle emission either and two that have were confirmed. Previously observed  $\beta$ -decay transitions and delayed  $\gamma$  rays have been measured to the highest statistical precision to date and with systematic uncertainties comparable to Refs. [15,16]. Using the  $\beta$ -decay intensity to the ground state from Armini *et al.* [13],  $\beta$ -delayed proton and alpha particle intensities from Honkanen *et al.* [31], and the  $\beta$ -decay intensities from the present work supplemented by  $\gamma$ -decay branching ratios from [8], the sum of the  $\beta$ -decay intensities was found to be 99.7(12)%, consistent with 100%. Figure 8 highlights the new energy levels and  $\gamma$ -ray transitions while displaying updated  $\gamma$ -ray transition probabilities and  $\beta$ -decay intensities. The newly observed photopeaks at 1659, 2775, 4954, 5798, 7484, and 8125 keV, as well as the newly observed escape peaks corresponding to the 8407-, 8861-, and 9207-keV photopeaks are displayed in Fig. 4. Table IV lists observed  $^{32}\text{S}$   $\gamma$  rays with their respective energies, initial and final states,

TABLE II. Partial widths and lifetimes for the  $^{32}\text{S}$  states at 8861 and 9651 keV.

$E_x$ (keV)	$\Gamma_p$ (eV)	$\Gamma_\alpha$ (eV)	$\Gamma_\gamma$ (eV)	$\tau$ (fs)
8861		0.0042(20)	0.0133(67)	38(17)
9650	0.21(7)	<0.0081	3.9(14)	0.16(5)

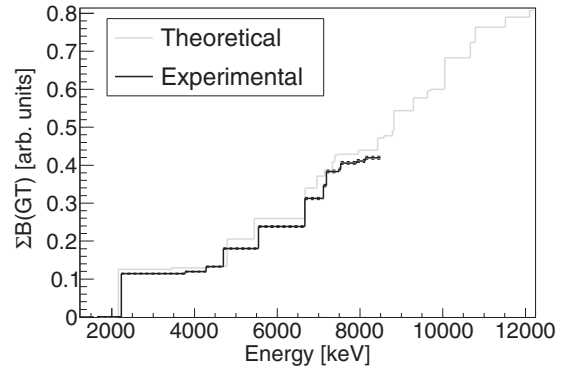


FIG. 10. Comparison of experimental and theoretical summed Gamow Teller strengths for the  $\beta$  decay of  $^{32}\text{Cl}$  to  $^{32}\text{S}$  states. The gray solid line represents the USDB theoretical values and the black solid line represents the experimental values with the corresponding uncertainties represented by black dashed lines. Due to the unknown mixing ratio, the  $B(\text{GT})$  value for the transition to the IAS was assumed to be zero and the transition to the 7190-keV state was assumed to be purely Gamow-Teller. The  $B(\text{GT})$  value for the transition to the ground state was calculated from the  $ft$  value adopted from [13].

and intensities, along with  $\beta$ -decay intensities, corresponding  $\log(ft)$  values, and uncertainties. Table IV also lists upper limits on the intensities of unobserved  $\gamma$  rays that were set in the present work.

Generally, the observed  $\gamma$ -ray transitions and  $\beta$ -decay intensities in the present work agree with, and build upon, those observed by Melconian *et al.* [15]. As a result, the  $ft$  values also agree with those determined reported in Ref. [15].

Construction of the coincidence matrix provided further evidence in support of the proposed decay scheme. 29 combinations of  $\gamma$ -ray transition were found to be in coincidence (Table I). This confirms and improves upon previous work [15,16], in which coincidences were not measured.

## B. Discussion of specific states

In previous works [15,16], the  $^{32}\text{Cl}$ -decay scheme deduced from observed transitions had to be supplemented by adopting data from nuclear reaction data for three  $\gamma$ -ray transitions [8]. One of the three supplemental transitions was observed in this analysis,  $1^+(9207) \rightarrow 0^+(\text{g.s.})$ . The other two transitions,  $1_4^+(8125) \rightarrow 2_1^+(2230)$  and  $0_4^+(7637) \rightarrow 2_2^+(4281)$ , were not observed in the present work either, but they are reported as upper limits, which improve upon previously reported upper limits [15].

### 1. 5006-keV state

The  $3^-$  state at 5006 keV was observed to be populated by a 1659-keV  $\gamma$ -ray transition from the 6666-keV  $^{32}\text{S}$  state. In particular, the 1659-keV  $\gamma$  ray was found to be in coincidence with the 2775-keV  $\gamma$  ray, which is known to deexcite the 5006-keV state. The intensity of the direct  $\beta$ -decay transition to the 5006-keV state was limited to be <0.053%, resulting in a corresponding limit of  $\log(ft) > 6.93$ . For comparison, Raman and Gove [33] have proposed the rule that the lower

TABLE III. Allowed  $^{32}\text{Cl}(\beta\gamma)^{32}\text{S}$  transitions from the present experiment and *sd* shell-model calculations (USDB and USDA). Spins, parities,  $^{32}\text{S}$  excitation energies  $E_x$ ,  $\beta$ -decay intensities  $I_\beta$ ,  $\log(ft)$  values, and Gamow Teller strengths  $B(\text{GT})$  are compiled. Experimental values are only shown for states with firm shell model identifications. Due to the unknown mixing ratio between the IAS and the 7190-keV states, their  $B(\text{GT})$  values are omitted from the table. The experimental values for the ground state are adopted from Ref. [13].

$J_n^\pi$	Experiment				USDB				USDA			
	$E_x$ (keV) [8]	$I_\beta(\%)$	$\log(ft)$	$B(\text{GT})$	$E_x$ (keV)	$I_\beta(\%)$	$\log(ft)$	$B(\text{GT})$	$E_x$ (keV)	$I_\beta(\%)$	$\log(ft)$	$B(\text{GT})$
$0_1^+$	0.0	$1.0^{+0.2}_{-0.5}$	$6.7^{+0.3}_{-0.1}$	0.0008(5)	0.0	0.43	7.053	0.0003	0.0	0.67	6.851	0.0005
$2_1^+$	2230.6	59.59(65)	4.521(5)	0.1134(13)	2160	59.18	4.492	0.1255	2173	58.84	4.481	0.1285
$0_2^+$	3778.4	1.14(6)	5.870(23)	0.0052(3)	3455	0.83	6.041	0.0035	3451	0.79	6.052	0.0034
$2_2^+$	4281.8	2.23(9)	5.443(14)	0.0134(5)	4378	0.58	5.953	0.0043	4387	0.57	5.951	0.0044
$1_1^+$	4695.3	5.80(15)	4.906(10)	0.0474(12)	4787	7.29	4.735	0.0716	4772	7.38	4.724	0.0734
$2_3^+$	5548.5	3.89(7)	4.819(12)	0.0581(11)	5446	3.47	4.852	0.0547	5441	3.43	4.848	0.0552
$2_4^+$	6666.1	1.97(5)	4.701(11)	0.0740(19)	6674	1.82	4.688	0.0798	6650	1.62	4.738	0.0712
$1_2^+$	7001.4	22.3(2)	3.508(4)	–	6840	24.54	3.490	–	6809	24.53	3.493	–
$2_5^+$	7115.3	0.588(25)	5.034(17)	0.0337(14)	6960	0.54	5.094	0.0313	6949	0.76	4.941	0.0446
$1_3^+$	7190.1	0.589(22)	5.01(2)	–	7149	0.23	5.391	–	7133	0.19	5.462	–
$0_3^+$	7535.7	0.183(11)	5.347(26)	0.0168(10)	7334	0.26	5.247	0.0220	7356	0.24	5.271	0.0209
$2_6^+$	7484.0	0.064(6)	5.83(5)	0.0056(5)	7396	0.20	5.331	0.0182	7379	0.19	5.345	0.0176
$0_4^+$	–	–	–	–	7460	0.020	6.308	0.0019	7461	0.035	6.051	0.0035
$0_5^+$	7921.0	0.037(7)	5.86(10)	0.0054(10)	7927	0.12	5.289	0.0019	7918	0.11	5.342	0.0035
$1_4^+$	8125.4	0.045(6)	5.65(6)	0.0084(11)	7959	0.06	5.560	0.0107	7927	0.07	6.471	0.0110
$2_7^+$	–	–	–	–	8044	0.13	5.207	0.0242	8048	0.12	5.209	0.0241
$2_8^+$	–	–	–	–	8422	0.11	5.055	0.3430	8397	0.12	5.020	0.0372
$0_6^+$	–	–	–	–	8432	0.0003	7.685	0.0001	8424	0.0002	7.722	0.0001
$2_9^+$	–	–	–	–	8578	0.014	5.846	0.0056	8567	0.015	5.812	0.0060
$2_{10}^+$	–	–	–	–	8781	0.024	5.487	0.0127	8768	0.022	5.529	0.0115
$1_5^+$	–	–	–	–	8821	0.09	4.863	0.0534	8813	0.09	4.885	0.0507
$0_7^+$	–	–	–	–	9293	0.027	5.060	0.0339	9286	0.025	5.093	0.0314
$1_7^+$	–	–	–	–	9633	0.007	5.331	0.0182	9590	0.008	5.307	0.0192
$1_8^+$	–	–	–	–	9716	0.0013	5.996	0.0039	9668	0.0016	5.940	0.0045
$1_9^+$	–	–	–	–	10051	0.012	4.667	0.0837	10018	0.014	4.656	0.0859
$1_{10}^+$	–	–	–	–	10669	0.0008	4.988	0.0400	10645	0.0008	5.050	0.0347
$0_8^+$	–	–	–	–	10789	0.0005	4.983	0.0405	10767	0.0005	5.015	0.0376

limit of the  $\log(ft)$  value for a first-forbidden unique transition such as this one is 8.5.

### 2. 5798-keV state

The energy of the observed 5798-keV  $\gamma$  ray is consistent with the energy of the only known transition from the  $1^-$   $^{32}\text{S}$  state at an excitation energy of 5797 keV (to the ground state). Therefore, we identified the observed  $\gamma$  ray with this transition. No other  $\gamma$  rays were observed to deexcite this state or feed it at our level of sensitivity. However, we are not able to exclude the possibility that this state is mainly populated by  $\beta\gamma$  decay rather than directly by a first-forbidden  $\beta$ -decay transition. The  $\beta$ -decay feeding was limited to be  $<0.036\%$ , corresponding to a limit of  $\log(ft) > 6.77$ .

### 3. 8407-keV state

The  $^{32}\text{S}$  state at 8407 keV was previously observed by Brenneisen *et al.* [34] via the  $^{29}\text{Si}(\alpha, n\gamma)$  reaction. However, only low energy  $\gamma$  rays were observed to deexcite this level in

that experiment due to an upper energy threshold for detection of approximately 6950 keV. In contrast, the only observed  $\gamma$ -ray transition deexciting this level in the present work was to the ground state. The  $\gamma$  rays that were observed in previous works were not observed in the present work and are reported as upper limits (Table IV). The previous work [34] found the following relative intensities: 20%, 18%, and 100% for the 3714-, 4126-, and 4625-keV  $\gamma$  rays, respectively. In the present work the following relative intensities were found:  $<139\%$ ,  $<50\%$ ,  $<159\%$ , and 100% for the 3714-, 4126-, 4625-, and 8407-keV  $\gamma$  rays, respectively. These present values are consistent with those from Ref. [34] with the exception of the new transition. Using  $\beta$ -decay selection rules the parity of the  $J = 2$ , 8407-keV state was determined to be positive for the first time.

### 4. 8861-keV state

The new information from the present work combined with data from past work enables us to calculate the lifetime and

TABLE IV.  $^{32}\text{Cl}$   $\beta$ -delayed  $\gamma$ -decay data from the present work, unless otherwise indicated.  $^{32}\text{S}$  energy levels, deduced spins and parities, calibrated  $\gamma$ -ray energies, transitions, intensities,  $\beta$ -decay intensities,  $\log ft$  values, and their respective uncertainties are shown.

Energy (keV)		Transition	$I_\gamma$ (%)		$I_\beta$ (%)	$\log ft$
$E_x - J_n^\pi$ [8,15]	$E_\gamma \pm \delta_{\text{stat}} \pm \delta_{\text{sys}}$		Melconian <i>et al.</i> [15]	Present work		
2230.6(2) - $2_1^+$	<sup>a</sup> 2230	$2_1^+(2230) \rightarrow 0^+(\text{g.s.})$	91.9 <sup>+0.6</sup> <sub>-0.4</sub>		59.59 $\pm$ 0.65	4.521 $\pm$ 0.005
3778.4(10) - $0_2^+$	<sup>a</sup> 1547	$0_2^+(3778) \rightarrow 2_1^+(2230)$	3.155 <sup>+0.040</sup> <sub>-0.036</sub>		1.14 $\pm$ 0.06	5.870 $\pm$ 0.023
	3779.6 $\pm$ 0.3 $\pm$ 0.7	$0_2^+(3778) \rightarrow 0^+(\text{g.s.})$	0.044 $\pm$ 0.025	0.044 $\pm$ 0.018		
4281.8(3) - $2_2^+$	2051.0 $\pm$ 0.0 $\pm$ 0.4	$2_2^+(4281) \rightarrow 2_1^+(2230)$	0.47 $\pm$ 0.04	0.419 $\pm$ 0.024	2.23 $\pm$ 0.09	5.443 $\pm$ 0.014
	<sup>a</sup> 4281	$2_2^+(4281) \rightarrow 0^+(\text{g.s.})$	2.42 $\pm$ 0.06			
4695.3(4) - $1_1^+$	916.8 $\pm$ 0.9 $\pm$ 0.4	$1_1^+(4695) \rightarrow 0_2^+(3778)$	0.034 $\pm$ 0.009	0.019 $\pm$ 0.006	5.80 $\pm$ 0.15	4.906 $\pm$ 0.010
	2464.6 $\pm$ 0.0 $\pm$ 0.5	$1_1^+(4695) \rightarrow 2_1^+(2230)$	4.24 $\pm$ 0.05	3.92 $\pm$ 0.12		
	<sup>a</sup> 4695	$1_1^+(4695) \rightarrow 0^+(\text{g.s.})$	2.42 $\pm$ 0.05			
5006.2(3) - $3_1^-$	726	$3_1^-(5006) \rightarrow 2_2^+(4281)$		<0.012	<0.053	>6.93
	1229	$3_1^-(5006) \rightarrow 0_2^+(3778)$		<0.015		
	<sup>d</sup> 2775.2 $\pm$ 0.2 $\pm$ 0.5	$3_1^-(5006) \rightarrow 2_1^+(2230)$		0.081 $\pm$ 0.009		
5548.5(10) - $2_3^+$	542	$2_3^+(5549) \rightarrow 3_1^-(5006)$		<0.009	3.89 $\pm$ 0.07	4.819 $\pm$ 0.012
	852.9 $\pm$ 0.4 $\pm$ 0.4	$2_3^+(5549) \rightarrow 1_1^+(4695)$	0.027 $\pm$ 0.008	0.014 $\pm$ 0.006		
	1266.9 $\pm$ 0.6 $\pm$ 0.4	$2_3^+(5549) \rightarrow 2_2^+(4281)$	<0.036 $\pm$ 0.013	0.022 $\pm$ 0.009		
	1769.8 $\pm$ 0.2 $\pm$ 0.4	$2_3^+(5549) \rightarrow 0_2^+(3778)$	0.136 $\pm$ 0.026	0.125 $\pm$ 0.013		
	<sup>a</sup> 3317	$2_3^+(5549) \rightarrow 2_1^+(2230)$	2.46 $\pm$ 0.05			
	<sup>a</sup> 5548	$2_3^+(5549) \rightarrow 0^+(\text{g.s.})$	1.50 <sup>+0.08</sup> <sub>-0.09</sub>			
5796.8(3) - $1_1^-$	<sup>d</sup> 5798.4 $\pm$ 0.9 $\pm$ 0.9	$1_1^-(5798) \rightarrow 0^+(\text{g.s.})$		0.028 $\pm$ 0.007	<0.036	>6.77
6666.1(10) - $2_4^+$	<sup>d</sup> 1659.9 $\pm$ 0.3 $\pm$ 0.4	$2_4^+(6666) \rightarrow 3_1^-(5006)$		0.040 $\pm$ 0.011	1.97 $\pm$ 0.05	4.701 $\pm$ 0.011
	1970.4 $\pm$ 0.2 $\pm$ 0.4	$2_4^+(6666) \rightarrow 1_1^+(4695)$	0.15 $\pm$ 0.04	0.134 $\pm$ 0.019		
	2383.6 $\pm$ 0.2 $\pm$ 0.5	$2_4^+(6666) \rightarrow 2_2^+(4281)$	0.077 <sup>+0.019</sup> <sub>-0.021</sub>	0.058 $\pm$ 0.007		
	<sup>a</sup> 2887	$2_4^+(6666) \rightarrow 0_2^+(3778)$	0.976 <sup>+0.028</sup> <sub>-0.025</sub>			
	4434.8 $\pm$ 0.0 $\pm$ 0.8	$2_4^+(6666) \rightarrow 2_1^+(2230)$	0.83 $\pm$ 0.06	0.730 $\pm$ 0.030		
	6664.9 $\pm$ 0.6 $\pm$ 1.5	$2_4^+(6666) \rightarrow 0^+(\text{g.s.})$	0.048 <sup>+0.018</sup> <sub>-0.019</sub>	0.036 $\pm$ 0.007		
7001.4(4) - $1_2^+$	1452.2 $\pm$ 0.1 $\pm$ 0.4	$1_2^+(7001) \rightarrow 2_3^+(5549)$	0.276 $\pm$ 0.019	0.235 $\pm$ 0.014	22.3 $\pm$ 0.2	3.508 $\pm$ 0.004
	2305.2 $\pm$ 0.1 $\pm$ 0.5	$1_2^+(7001) \rightarrow 1_1^+(4695)$	0.137 $\pm$ 0.023	0.157 $\pm$ 0.009		
	2718.8 $\pm$ 0.0 $\pm$ 0.5	$1_2^+(7001) \rightarrow 2_2^+(4281)$	0.533 <sup>+0.019</sup> <sub>-0.024</sub>	0.471 $\pm$ 0.017		
	3222.1 $\pm$ 0.0 $\pm$ 0.6	$1_2^+(7001) \rightarrow 0_2^+(3778)$	0.881 <sup>+0.029</sup> <sub>-0.027</sub>	0.764 $\pm$ 0.025		
	<sup>a</sup> 4769.8 $\pm$ 0.0 $\pm$ 0.9	$1_2^+(7001) \rightarrow 2_1^+(2230)$	20.62 <sup>+0.20</sup> <sub>-0.17</sub>			
	7000.6 $\pm$ 0.3 $\pm$ 1.5	$1_2^+(7001) \rightarrow 0^+(\text{g.s.})$	0.057 $\pm$ 0.016	0.054 $\pm$ 0.007		
7115.3(10) - $2^+$	2107	$2^+(7115) \rightarrow 3_1^-(5006)$		<0.010	0.588 $\pm$ 0.025	5.034 $\pm$ 0.017
	2418.3 $\pm$ 0.2 $\pm$ 0.5	$2^+(7115) \rightarrow 1_1^+(4695)$	0.057 <sup>+0.013</sup> <sub>-0.015</sub>	0.064 $\pm$ 0.009		
	2831.0 $\pm$ 0.7 $\pm$ 0.5	$2^+(7115) \rightarrow 2_2^+(4281)$	0.019 $\pm$ 0.013	0.022 $\pm$ 0.008		
	3339.0 $\pm$ 0.4 $\pm$ 0.7	$2^+(7115) \rightarrow 0_2^+(3778)$	0.037 $\pm$ 0.015	0.024 $\pm$ 0.009		
	4882.7 $\pm$ 0.0 $\pm$ 0.9	$2^+(7115) \rightarrow 2_1^+(2230)$	0.504 <sup>+0.031</sup> <sub>-0.032</sub>	0.477 $\pm$ 0.020		
	7115	$2^+(7115) \rightarrow 0^+(\text{g.s.})$		<0.020		
7190.1(15) - $1_3^+$	2183	$1_3^+(7190) \rightarrow 3_1^-(5006)$		<0.010	0.589 $\pm$ 0.022	5.01 $\pm$ 0.02
	2911	$1_3^+(7190) \rightarrow 2_2^+(4281)$		<0.030		
	2494.4 $\pm$ 0.8 $\pm$ 0.5	$1_3^+(7190) \rightarrow 1_1^+(4695)$	0.016 $\pm$ 0.014	0.010 $\pm$ 0.007		
	3412.5 $\pm$ 0.1 $\pm$ 0.7	$1_3^+(7190) \rightarrow 0_2^+(3778)$	0.122 $\pm$ 0.019	0.148 $\pm$ 0.012		
	4958.7 $\pm$ 0.1 $\pm$ 0.9	$1_3^+(7190) \rightarrow 2_1^+(2230)$	0.32 $\pm$ 0.04	0.262 $\pm$ 0.014		
	<sup>a</sup> 7190	$1_3^+(7190) \rightarrow 0^+(\text{g.s.})$	0.169 <sup>+0.024</sup> <sub>-0.020</sub>			
7484.0(4) - $2_6^+$	2480	$2_6^+(7484) \rightarrow 3_1^-(5006)$		<0.070	0.064 $\pm$ 0.006	5.83 $\pm$ 0.05
	3203	$2_6^+(7484) \rightarrow 2_2^+(4281)$		<0.006		
	<sup>d</sup> 7483.7 $\pm$ 0.3 $\pm$ 1.5	$2_6^+(7484) \rightarrow 0^+(\text{g.s.})$		0.064 $\pm$ 0.006		
7535.7(10) - $0_3^+$	2839.7 $\pm$ 0.1 $\pm$ 0.5	$0_3^+(7536) \rightarrow 1_1^+(4695)$	0.185 $\pm$ 0.018	0.183 $\pm$ 0.011	0.183 $\pm$ 0.011	5.347 $\pm$ 0.026
	5304	$0_3^+(7536) \rightarrow 2_1^+(2230)$		<0.031		
	7534	$0_3^+(7536) \rightarrow 0^+(\text{g.s.})$		<0.042		
7637.0(10) - $0_4^+$	3355	$0_4^+(7637) \rightarrow 2_2^+(4281)$		<0.028		
7921.0(10) - $0^+$	5691.6 $\pm$ 0.7 $\pm$ 0.9	$0_4^+(7921) \rightarrow 2_1^+(2230)$	0.033 <sup>+0.014</sup> <sub>-0.013</sub>	0.037 $\pm$ 0.007	0.037 $\pm$ 0.007	5.86 $\pm$ 0.10

TABLE IV. (*Continued.*)

Energy (keV)		Transition	$I_\gamma$ (%)		$I_\beta$ (%)	$\log ft$
$E_x - J_n^\pi$ [8,15]	$E_\gamma \pm \delta_{\text{stat}} \pm \delta_{\text{sys}}$		Melconian <i>et al.</i> [15]	Present work		
8125.4(2) - $1_4^+$	3120	$1_4^+(8125) \rightarrow 3_1^-(5006)$		<0.015	$0.045 \pm 0.006$	$5.65 \pm 0.06$
	5895	$1_4^+(8125) \rightarrow 2_1^+(2230)$		<0.015		
	<sup>d</sup> $8125.4 \pm 0.4 \pm 1.5$	$1_4^+(8125) \rightarrow 0^+(\text{g.s.})$		$0.045 \pm 0.006$		
8407.0(14) - $2^+$	3400	$2^+(8407) \rightarrow 3_1^-(5006)$		<0.012	$0.033 \pm 0.005$	$5.6 \pm 0.1$
	3714 <sup>c</sup>	$2^+(8407) \rightarrow 1_1^+(4695)$		<0.045		
	4126 <sup>c</sup>	$2^+(8407) \rightarrow 2_2^+(4281)$		<0.016		
	4625 <sup>c</sup>	$2^+(8407) \rightarrow 0_2^+(3778)$		<0.052		
	<sup>d</sup> $8406.7 \pm 0.3 \pm 1.5$	$2^+(8407) \rightarrow 0^+(\text{g.s.})$		$0.033 \pm 0.005$		
8861(2) - $2^+$	3858	$2^+(8861) \rightarrow 3_1^-(5006)$		<0.013	$0.061^e \pm 0.011$	$5.07 \pm 0.05$
	6630	$2^+(8861) \rightarrow 2_1^+(2230)$		<0.012		
	<sup>d</sup> $8859.8 \pm 0.5 \pm 1.5$	$2^+(8861) \rightarrow 0^+(\text{g.s.})$		$0.024 \pm 0.005$		
9207.6(7) - $1^+$	$6973.3 \pm 0.2 \pm 1.5$	$1^+(9207) \rightarrow 2_1^+(2230)$	$0.098 \pm 0.018$	$0.015 \pm 0.004$	$0.047^e \pm 0.007$	$4.93 \pm 0.06$
	<sup>d</sup> $9207.3 \pm 1.1 \pm 1.5$	$1^+(9207) \rightarrow 0^+(\text{g.s.})$		$0.016 \pm 0.005$		
9650.2(5) - $2^+$	4101	$2^+(9650) \rightarrow 2_3^+(5549)$		<0.038	$0.102^e \pm 0.015$	$4.23 \pm 0.06$
	4643	$2^+(9650) \rightarrow 3_1^-(5006)$		<0.015		
	<sup>d</sup> $4954.2 \pm 0.55 \pm 0.9$	$2^+(9650) \rightarrow 1_1^+(4695)$		$0.038 \pm 0.008$		
	5368	$2^+(9650) \rightarrow 2_2^+(4281)$		<0.018		
	5871	$2^+(9650) \rightarrow 0_2^+(3778)$		<0.004		
	7419	$2^+(9650) \rightarrow 2_1^+(2230)$		<sup>b</sup> $0.055 \pm 0.008$		

<sup>a</sup>Data used as input to efficiency calibration; therefore energies and  $\gamma$ -ray intensities were not determined independently.

<sup>b</sup>Data adopted from ENSDF [8].

<sup>c</sup>Not observed: upper limits for transitions that were previously observed in reaction experiments, but were not observed in the present work.

<sup>d</sup> $\gamma$ -ray transitions that have been observed for the first time, from  $^{32}\text{Cl}(\beta\gamma)^{32}\text{S}$ , in the present work.

<sup>e</sup>Includes unobserved  $\beta$ - $\alpha$ ,  $\beta$ - $p$ , and  $\beta$ - $\gamma$ -decay branches, not explicitly shown in the table, that were adopted from ENSDF [8] or Honkanen *et al.* [31] to find the total  $\beta$ -decay intensity feeding the state.

partial widths for this state. Our  $\beta$ -delayed  $\gamma$ -decay intensity is 0.024(5)% for the 8861-keV  $\gamma$  ray, which is the only one observed. Including the other  $\gamma$  branches from ENSDF [8] increases the total  $\beta$ - $\gamma$  intensity to 0.046(11)%. From Honkanen *et al.* [31] the  $\beta$ - $\alpha$  intensity is 0.0146(20)%. Comparing the  $\beta$ - $\alpha$  intensity to the  $\beta$ - $\gamma$  intensity gives the branching ratios. The proton width for this state is negligibly small due to its close proximity to the proton threshold and the Coulomb barrier. The resonance strength for the  $^{28}\text{Si}(\alpha, \gamma)^{32}\text{S}$  reaction as defined and measured by Rogers *et al.* [35] is 16(3) meV. The spin of the level is 2 from ENSDF. Using this information, the total width of the state is 17.5(77) meV, corresponding to a lifetime of 38(17) fs. From this and the branching ratios, one can calculate the partial widths for  $\alpha$  and  $\gamma$  emission (Table II).

### 5. 9207-keV state

In the present work the 9207-keV  $\gamma$  ray decaying from the 9207-keV  $^{32}\text{S}$  state has a relative intensity of 100(32)%, while the 6973-keV  $\gamma$  ray decaying from the same state has a relative intensity of 96(26)%. This is consistent with experimental nuclear reaction experiments [8,36], which have yielded relative intensities of 100(6)% and 99(6)% for the 9207- and 6973-keV  $\gamma$  rays, respectively.

The  $\beta\gamma$  intensity of 0.015(4)% for the 6973-keV  $\gamma$  ray measured in the present experiment is significantly lower than

the value of 0.098(18)% reported in the most recent  $^{32}\text{Cl}$   $\beta$ -decay experiment [15]. The difference can be attributed to a contribution to the 6973-keV peak from the first-escape peak of the 7484-keV photopeak, which was not detected in the previous experiment.

### 6. 9650-keV state

Placing the newly observed 4954-keV  $\gamma$  ray in the decay scheme required some interpretation because the low statistics for the corresponding peak rendered  $\gamma$ - $\gamma$  coincidences unobservable. Based on energy considerations, candidate initial  $^{32}\text{S}$  states for the 4954-keV  $\gamma$  ray include the 8729-, the 8737-, and the 9650-keV states. The 8729-keV state has a spin and parity of  $3^+$ , which should not be directly populated via  $\beta$  decay and should not have a strong  $\gamma$ -ray branch to the  $0^+$  state at 3778 keV. Adding the 4954-keV  $\gamma$ -ray energy to the excitation energy of the 3775-keV state yields an excitation energy of 8733 keV, which is 4 keV away from both the 8729- and 8737-keV states. On the other hand, adding 4954 keV to the excitation energy of the 4695-keV state yields the excitation energy of the known state at 9650 keV.  $^{32}\text{Cl}$   $\beta$ -delayed proton emission experiments [8,36] have also observed population of the 9650-keV state. Therefore, the newly observed 4954-keV  $\gamma$  ray was interpreted to be from the 9650-keV state.

The 9650-keV state has a previously known 7419-keV  $\gamma$ -ray transition to the first excited state [8] that was near our detection sensitivity threshold, and it was, therefore, not detected definitively. Instead, we adopted the relative intensity value from ENSDF, assigning the 7419-keV  $\gamma$  ray a relative intensity of 100(9)%, while the newly observed 4954-keV  $\gamma$  ray decaying from the 9650-keV  $^{32}\text{S}$  state was assigned a relative intensity of 69(6)%.

The new information from the present work combined with data from past work enables us to calculate the lifetime and partial widths for this state. Our  $\beta$ -delayed  $\gamma$ -decay intensity is 0.038(8)% for the 4954-keV  $\gamma$  ray, which is the only one observed. Including the other  $\gamma$  branches from ENSDF [8] increases the  $\beta$ - $\gamma$  intensity to 0.097(15)%. From Honkanen *et al.* [31] the  $\beta$ - $p$  intensity is 0.0052(8)% and the upper limit on the  $\beta$ - $\alpha$  intensity is  $<0.0002\%$ . Comparing the  $\beta$ - $p$  and  $\beta$ - $\alpha$  intensities to the  $\beta$ - $\gamma$  branch gives the branching ratios. The resonance strength for the  $^{31}\text{P}(p, \gamma)^{32}\text{S}$  reaction as defined and evaluated by Iliadis *et al.* [37] is 0.25(2) eV. The spin of the level is 2 from ENSDF. The spins of  $^{31}\text{P}$  and the proton are both 1/2. Using this information, the total width of the state is 4.1(13) eV, corresponding to a lifetime of 0.16(5) fs. From this and the branching ratios, one can calculate the partial widths for proton and  $\gamma$  emission and impose a strong upper limit on the partial width for  $\alpha$  emission (Table II).

The proton width and the upper limit on the alpha width can be used to calculate an upper limit on the resonance strength (as defined in Ref. [37]) for the  $^{31}\text{P}(p, \alpha)^{28}\text{Si}$  reaction of  $\omega\gamma < 9.8$  meV. This limit is more stringent than the one set by Kuperus *et al.* [38] by direct measurements confirming that, although this resonance is in the Gamow window for explosive thermonuclear hydrogen burning in some astrophysical environments, it is not strong enough to be important in comparison to other resonances.

### C. Comparison to shell model

Calculations were carried out in the  $sd$  shell model space with the USDA and USDB Hamiltonians from [39] added with the Coulomb and charge-dependent interactions from [40]. The results are similar to those given in [15]. The GT+ decay up to 8 MeV contains about 9% of the total strength. The quenching factor of 0.6 as obtained from the average in the  $sd$  shell [41] was used for the theoretical  $B(\text{GT})$  values. The difference between USDA and USDB shown in Table III gives a measure of the uncertainty coming from the Hamiltonian.

Experimental values for  $B(\text{GT})$  were calculated using Eq. (7) in Ref. [15]. The  $ft$  values from the present work were used together with a value of  $\mathcal{F}_t^{0^+ \rightarrow 0^+} = 3072.27(62)$  from the survey of Hardy and Towner [1] and the values of  $\delta'_R$  for the transition-dependent part of the radiative correction adopted from Ref. [15].

The experimental  $B(\text{GT})$  values are compared to the theoretical values in Table III and Fig. 10. The detailed state-by-state agreement between experiment and theory is good. The strength of the allowed Gamow-Teller transition to the  $^{32}\text{S}$  ground state is very weak and consistent with the 90% C.L. upper limit of 2.2 % deduced from the sum of the  $\beta$ -decay intensities from the present experiment and the constraint that they must sum to 100%.

An interesting anomaly is the 6582(5)-keV state [8], which was not observed in the present work. In a previous evaluation [8], the 6582(5)-keV state was determined to have an ambiguous  $J^\pi = (2^+, 3^-)$ . All of the observed bound states with  $J^\pi = 2^+$  could be matched with those predicted by the  $sd$  shell model based on a comparison of their  $\beta$ -decay feedings and  $\gamma$ -decay branchings, yielding a clear one-to-one correspondence without the 6582-keV state. If the 6582-keV state has  $J^\pi = 2^+$ , then it must be an intruder state considering that all of the  $sd$  shell states have been identified. However, based on the apparently weak  $\beta$  feeding of this state, we conclude that the spin and parity is more likely to be  $3^-$  than  $2^+$  since the latter would correspond to an observable allowed transition.

One might ask whether the  $^{32}\text{S}$  states populated in allowed  $^{32}\text{Cl}$   $\beta$ -decay transitions are predicted by the  $sd$  shell model to have observable  $\gamma$ -decay branches to positive parity  $^{32}\text{S}$  states with spin higher than 2. The shell model predicts that any such branches would have been beyond the sensitivity of the present experiment, consistent with their nonobservation. In particular, the 2207-keV transition from the  $2^+$  state at 6666 keV to the  $4^+$  state at 4459 keV is predicted to have an intensity of approximately 0.01%, which might have been detectable if the photopeak were not at essentially the same energy as the first-escape peak of the 2719-keV  $\gamma$  ray.

## V. CONCLUSION

The present experiment has produced the most sensitive  $^{32}\text{Cl}$   $\beta$ -delayed  $\gamma$ -ray data set to date, providing a more detailed decay scheme that was verified using  $\gamma$ - $\gamma$  coincidences. Nine previously unobserved  $\beta$ -delayed  $\gamma$ -ray transitions were detected leading to the inference of  $\beta$ -decay transitions to five  $^{32}\text{S}$  states that have not been observed via  $\beta$ -delayed  $\gamma$  decay before. Furthermore, the parity of the  $^{32}\text{S}$  state at 8407 keV was determined to be positive, the lifetimes and partial widths of the 8861- and 9650-keV states were determined, and arguments were presented that the 6582-keV state is unlikely to have a spin and parity of  $2^+$ . The decay scheme is in good agreement with  $sd$  shell model calculations.

All allowed  $^{32}\text{Cl}$   $\beta$ -decay transitions to bound positive parity  $^{32}\text{S}$  states with  $J \leq 2$  predicted by the  $sd$  shell model were observed. In addition, the (potentially indirect) population of the lowest  $3^-$  and  $1^-$  states in  $^{32}\text{S}$  was observed, corresponding to at least half of the known bound negative parity states of  $^{32}\text{S}$  with  $J \leq 3$ . This broader population of states through  $\beta$  and  $\beta\gamma$  feeding hints at the prospect for using  $\beta$  decay to perform complete spectroscopy measurements at the next generation of radioactive beam facilities, where beam intensities will be several orders of magnitude higher. The corresponding increase in activity associated with forbidden  $\beta$ -decay transitions and weak  $\gamma$  transitions will provide sensitivity to a set of states with an even broader range of spins and parities than the present work, approaching complete spectroscopy despite the inherent selectivity of the  $\beta$ -decay process.

## ACKNOWLEDGMENTS

The authors gratefully acknowledge the NSCL operations staff for providing the  $^{32}\text{Cl}$  beam. This work was supported

by the US National Science Foundation under Grants No. PHY-1102511, No. PHY-1404442, No. PHY-1419765, and No. PHY-1431052; by the US Department of Energy, Office of Science under Grant No. DE-SC00106052; by the National Nuclear Security Administration under Grant No.

DE-NA0000979; and by the Natural Sciences and Engineering Research Council of Canada. E.A. acknowledges support from the Lawrence W. Hantel Endowed Fellowship Fund, in Memory of Prof. Donald J. Montgomery.

- 
- [1] J. C. Hardy and I. S. Towner, *Phys. Rev. C* **91**, 025501 (2015).
- [2] A. Saastamoinen, L. Trache, A. Banu, M. A. Bentley, T. Davinson, J. C. Hardy, V. E. Jacob, M. McCleskey, B. T. Roeder, E. Simmons, G. Tabacaru, R. E. Tribble, P. J. Woods, and J. Äystö, *Phys. Rev. C* **83**, 045808 (2011).
- [3] J. P. Wallace, P. J. Woods, G. Lotay, A. Alharbi, A. Banu, H. M. David, T. Davinson, M. McCleskey, B. T. Roeder, E. Simmons, A. Spiridon, L. Trache, and R. E. Tribble, *Phys. Lett. B* **712**, 59 (2012).
- [4] E. Pollacco, L. Trache, E. Simmons, A. Spiridon, M. McCleskey, B. T. Roeder, A. Saastamoinen, R. E. Tribble, G. Pascovici, M. Kebbiri, J. P. Mols, and M. Raillot, *Nucl. Instrum. Methods Phys. Res., Sect. A* **723**, 102 (2013).
- [5] M. B. Bennett, C. Wrede, K. A. Chipps, J. José, S. N. Liddick, M. Santia, A. Bowe, A. A. Chen, N. Cooper, D. Irvine *et al.*, *Phys. Rev. Lett.* **111**, 232503 (2013).
- [6] M. B. Bennett, C. Wrede, B. A. Brown, S. N. Liddick, D. Pérez-Loureiro, D. W. Bardayan, A. A. Chen, K. A. Chipps, C. Fry, B. E. Glassman, C. Langer, N. R. Larson, E. I. McNeice, Z. Meisel, W.-J. Ong, P. D. O'Malley, S. D. Pain, C. J. Prokop, H. Schatz, S. B. Schwartz, S. Suchyta, P. Thompson, M. Walters, and X. Xu, *Phys. Rev. Lett.* **116**, 102502 (2016).
- [7] C. Wrede, B. E. Glassman, D. Pérez-Loureiro, J. M. Allen, D. W. Bardayan, M. B. Bennett, B. A. Brown, K. A. Chipps, M. Febraro, C. Fry, M. R. Hall, O. Hall, S. N. Liddick, P. O'Malley, W.-J. Ong, S. D. Pain, S. B. Schwartz, P. Shidling, H. Sims, P. Thompson, and H. Zhang, *Phys. Rev. C* **96**, 032801 (2017).
- [8] C. Ouellet and B. Singh, *Nucl. Data Sheets* **112**, 2199 (2011).
- [9] G. Audi, F. G. Kondev, M. Wang, B. Pfeiffer, X. Sun, J. Blachot, and M. MacCormick, *Chin. Phys. C* **36**, 1157 (2012).
- [10] S. W. Breckon, A. Henrikson, J. S. Foster, and W. M. Martin, *Can. J. Phys.* **32**, 223 (1954).
- [11] N. W. Glass and J. R. Richardson, *Phys. Rev.* **98**, 1251 (1955).
- [12] W. Anderson, L. Dillman, and J. Kraushaar, *Nucl. Phys.* **77**, 401 (1966).
- [13] A. J. Armini, J. W. Sunier, and J. R. Richardson, *Phys. Rev.* **165**, 1194 (1968).
- [14] C. Détraz, C. Zaid, D. Frantsvog, R. Wilson, and A. Kunselman, *Nucl. Phys. A* **203**, 414 (1973).
- [15] D. Melconian, S. Triambak, C. Bordeanu, A. García, J. C. Hardy, V. E. Jacob, N. Nica, H. I. Park, G. Tabacaru, L. Trache, I. S. Towner, R. E. Tribble, and Y. Zhai, *Phys. Rev. C* **85**, 025501 (2012).
- [16] D. Melconian, S. Triambak, C. Bordeanu, A. García, J. C. Hardy, V. E. Jacob, N. Nica, H. I. Park, G. Tabacaru, L. Trache, I. S. Towner, R. E. Tribble, and Y. Zhai, *Phys. Rev. Lett.* **107**, 182301 (2011).
- [17] I. S. Towner and J. C. Hardy, *Phys. Rev. C* **82**, 065501 (2010).
- [18] K. Kaneko, Y. Sun, T. Mizusaki, S. Tazaki, and S. K. Ghorui, *Phys. Lett. B* **773**, 521 (2017).
- [19] M. B. Bennett, C. Wrede, S. N. Liddick, D. Pérez-Loureiro, D. W. Bardayan, B. A. Brown, A. A. Chen, K. A. Chipps, C. Fry, B. E. Glassman, C. Langer, N. R. Larson, E. I. McNeice, Z. Meisel, W. Ong, P. D. O'Malley, S. D. Pain, C. J. Prokop, H. Schatz, S. B. Schwartz, S. Suchyta, P. Thompson, M. Walters, and X. Xu, *Phys. Rev. C* **97**, 065803 (2018).
- [20] M. B. Bennett, C. Wrede, B. A. Brown, S. N. Liddick, D. Pérez-Loureiro, D. W. Bardayan, A. A. Chen, K. A. Chipps, C. Fry, B. E. Glassman, C. Langer, N. R. Larson, E. I. McNeice, Z. Meisel, W.-J. Ong, P. D. O'Malley, S. D. Pain, C. J. Prokop, S. B. Schwartz, S. Suchyta, P. Thompson, M. Walters, and X. Xu, *Phys. Rev. C* **93**, 064310 (2016).
- [21] D. Pérez-Loureiro, C. Wrede, M. B. Bennett, S. N. Liddick, A. Bowe, B. A. Brown, A. A. Chen, K. A. Chipps, N. Cooper, D. Irvine *et al.*, *Phys. Rev. C* **93**, 064320 (2016).
- [22] S. B. Schwartz, C. Wrede, M. B. Bennett, S. N. Liddick, D. Pérez-Loureiro, A. Bowe, A. A. Chen, K. A. Chipps, N. Cooper, D. Irvine *et al.*, *Phys. Rev. C* **92**, 031302 (2015).
- [23] D. Pérez-Loureiro, C. Wrede, M. B. Bennett, S. N. Liddick, A. Bowe, B. A. Brown, A. A. Chen, K. A. Chipps, N. Cooper, E. McNeice, F. Naqvi, R. Ortez, S. D. Pain, J. Pereira, C. Prokop, S. J. Quinn, J. Sakstrup, M. Santia, S. B. Schwartz, S. Shanab, A. Simon, A. Spyrou, and E. Thiagalingam, *Phys. Rev. C* **96**, 014306 (2017).
- [24] B. E. Glassman, D. Pérez-Loureiro, C. Wrede, J. Allen, D. W. Bardayan, M. B. Bennett, B. A. Brown, K. A. Chipps, M. Febraro, C. Fry *et al.*, *Phys. Rev. C* **92**, 042501 (2015).
- [25] B. E. Glassman, D. Pérez-Loureiro, C. Wrede, J. Allen, D. W. Bardayan, M. B. Bennett, B. A. Brown, K. A. Chipps, M. Febraro, M. Friedman, C. Fry, M. R. Hall, O. Hall, S. N. Liddick, P. O'Malley, W. J. Ong, S. D. Pain, C. Prokop, S. B. Schwartz, P. Shidling, H. Sims, P. Thompson, and H. Zhang, *Phys. Lett. B* **778**, 397 (2018).
- [26] D. Morrissey, B. Sherrill, M. Steiner, A. Stolz, and I. Wiedenhoever, *Nucl. Instrum. Methods Phys. Res., Sect. B* **204**, 90 (2003).
- [27] D. Bazin, V. Andreev, A. Becerril, M. Doléans, P. Mantica, J. Ottarson, H. Schatz, J. Stoker, and J. Vincent, *Nucl. Instrum. Methods Phys. Res., Sect. A* **606**, 314 (2009).
- [28] C. Prokop, S. Liddick, B. Abromeit, A. Chemey, N. Larson, S. Suchyta, and J. Tompkins, *Nucl. Instrum. Methods Phys. Res., Sect. A* **741**, 163 (2014).
- [29] G. R. Gilmore, *Practical Gamma-Ray Spectrometry* (Wiley, New York, 2008), p. 361.
- [30] S. Agostinelli *et al.*, *Nucl. Instrum. Methods Phys. Res., Sect. A* **506**, 250 (2003).
- [31] J. Honkanen, M. Kortelahti, K. Valli, K. Eskola, A. Hautojärvi, and K. Vierinen, *Nucl. Phys. A* **330**, 429 (1979).
- [32] B. A. Brown, *Prog. Part. Nucl. Phys.* **47**, 517 (2001).
- [33] S. Raman and N. B. Gove, *Phys. Rev. C* **7**, 1995 (1973).
- [34] J. Brenneisen, B. Erhardt, F. Glatz, T. Kern, R. Ott, H. Ropke, J. Schmalzlin, P. Siedle, and B. H. Wildenthal, *Z. Phys. A: Hadrons Nucl.* **357**, 157 (1997).

- [35] D. W. O. Rogers, W. R. Dixon, and R. S. Storey, *Nucl. Phys. A* **281**, 345 (1977).
- [36] W. Coetzee, M. Meyer, and D. Reitmann, *Nucl. Phys. A* **185**, 644 (1972).
- [37] C. Iliadis, J. M. D'Auria, S. Starrfield, W. J. Thompson, and M. Wiescher, *Astrophys. J. Suppl. Ser.* **134**, 151 (2001).
- [38] J. Kuperus, P. W. M. Glaudemans, and P. M. Endt, *Physica* **29**, 1281 (1963).
- [39] B. A. Brown and W. A. Richter, *Phys. Rev. C* **74**, 034315 (2006).
- [40] W. E. Ormand and B. A. Brown, *Nucl. Phys. A* **491**, 1 (1989).
- [41] W. A. Richter, S. Mkhize, and B. A. Brown, *Phys. Rev. C* **78**, 064302 (2008).